

Two-dimensional dopant profiling by electrostatic force microscopy using carbon nanotube modified cantilevers

This content has been downloaded from IOPscience. Please scroll down to see the full text.

2008 Nanotechnology 19 325703

(<http://iopscience.iop.org/0957-4484/19/32/325703>)

View [the table of contents for this issue](#), or go to the [journal homepage](#) for more

Download details:

IP Address: 140.113.38.11

This content was downloaded on 25/04/2014 at 15:19

Please note that [terms and conditions apply](#).

Two-dimensional dopant profiling by electrostatic force microscopy using carbon nanotube modified cantilevers

Shu-Cheng Chin¹, Yuan-Chih Chang¹, Chen-Chih Hsu²,
Wei-Hsiang Lin³, Chih-I Wu², Chia-Seng Chang¹, Tien T Tsong^{1,3},
Wei-Yen Woon⁴, Li-Te Lin⁴ and Hun-Jan Tao⁴

¹ Institute of Physics, Academia Sinica, Taipei 115, Taiwan, Republic of China

² Institute of Photonics and Optoelectronics, National Taiwan University, Taipei 106, Taiwan, Republic of China

³ Institute of Electrophysics, National Chiao Tung University, Hsinchu 300, Taiwan, Republic of China

⁴ Taiwan Semiconductor Manufacturing Company, Hsinchu 300, Taiwan, Republic of China

E-mail: jasonc@phys.sinica.edu.tw

Received 15 April 2008, in final form 2 June 2008

Published 4 July 2008

Online at stacks.iop.org/Nano/19/325703

Abstract

A two-dimensional (2D) dopant profiling technique is demonstrated in this work. We apply a unique cantilever probe in electrostatic force microscopy (EFM) modified by the attachment of a multiwalled carbon nanotube (MWNT). Furthermore, the tip apex of the MWNT was trimmed to the sharpness of a single-walled carbon nanotube (SWNT). This ultra-sharp MWNT tip helps us to resolve dopant features to within 10 nm in air, which approaches the resolution achieved by ultra-high vacuum scanning tunnelling microscopy (UHV STM). In this study, the CNT-probed EFM is used to profile 2D buried dopant distribution under a nano-scale device structure and shows the feasibility of device characterization for sub-45 nm complementary metal–oxide–semiconductor (CMOS) field-effect transistors.

1. Introduction

As we continue to scale down electronic devices and approach the sub-nanometre range, well-controlled and uniform device performance is getting harder to achieve. In particular, the control of its effective channel length (L_{eff}) and consistent threshold voltage in a static random access memory (SRAM) remains one of the major challenges [1]. Due to the induced transient dopant diffusion during device processing such as thermal annealing, mechanical polishing, dry/wet etching, and so on, the large variation of dopant profile under a poly-silicon gate could undermine the eventual drive current/threshold voltage performance of a transistor array [2–4]. In order to clarify these issues and to develop process solutions, a practical and convenient methodology for two-dimensional (2D) plane view dopant profiling is urgently needed.

According to the International Technology Roadmap for Semiconductors (ITRS Roadmap), a dopant profiling methodology is required to achieve 1.5 nm spatial resolution

and 3% dopant concentration accuracy for device technology under 100 nm [5]. Among all the candidates, scanning spreading resistance microscopy (SSRM), first developed by IMEC in 1994, has been shown capable of achieving such criteria in cross-sectioned samples [6]. The SSRM employs a strong tip pressure up to GPa and thus is destructive to both the sample surface and the scanning tip [7–9]. In a more global view, to gain control of the drive current uniformity and threshold voltage variation, a two-dimensional plane view methodology is required. Unfortunately, the back contact fabrication for SSRM is extremely difficult for the plane view sample. The Fujitsu Corporation has succeeded in the plane view detection of a 2D effective channel length under a poly-silicon gate, using ultra-high vacuum scanning tunnelling microscopy (UHV STM) after proper de-layering [10–12]. They observed with high resolution the L_{eff} variation induced by the shallow trench isolation (STI) stress, and its dependence on the device pattern. So far, this is the only plane view dopant profiling in nanometres reported [10]. Nevertheless, the

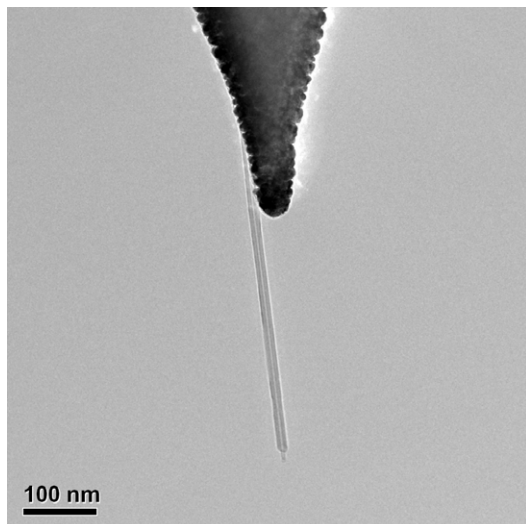


Figure 1. The TEM image of our CNT-modified cantilevers, showing that the contact between the CNT and PtIr coated tip surface appears clean and the apex is sharpened to 5 nm by *in situ* trimming in the UHV TEM chamber.

sample preparation in a UHV STM requires repeated flashing of the sample to a very high temperature ~ 1400 K, which could disturb the original dopant distribution and thus produce data not close to the process condition.

Electrostatic force microscopy (EFM) [13, 14] and scanning capacitance microscopy (SCM) [15–17] are alternative non-contact, ambient scanning probe options for achieving the above goal. For the SCM, a uniform oxide layer, usually formed by ultraviolet (UV) lamp treatment, is grown to ensure no artefacts from oxide inhomogeneities or impurities. The spatial resolution is limited by both the capacitive oxide and the tip size. For the EFM case, although there is no need for additional growth of an oxide layer, the spatial resolution is generally limited by operating at a farther distance from the sample in the secondary scan.

2. Carbon nanotube modified cantilevers

It has been reported that applying a carbon nanotube (CNT) tip in atomic force microscopy (AFM) can significantly increase the imaging resolution [18, 19]. In the late 1990s, EFM with a resolution of 5 nm was first reported using CNT-modified cantilevers [20–22]. Conventionally, fabrication of a CNT-modified cantilever is performed with an optical microscope (OM). Due to the limited resolution of OMs, it is often hard to tell whether the CNT is really attached to the cantilever or not. It becomes even more difficult when we attempt to control the CNT's size and shape. To improve the situation, a scanning electron microscope (SEM) is usually employed instead. However, the fabricated tips are often contaminated because of the poor vacuum conditions ($\sim 10^{-6}$ Torr) in a SEM chamber.

In this paper, we develop a new technique by modifying the AFM cantilever with a trimmed multiwalled carbon nanotube (MWNT). The MWNT, 15 nm in diameter and

300 nm in length, shown in figure 1, is chosen and attached to a commercial PtIr/Cr coated n^+ -Si cantilever, NANOSensors PointProbe EFM, inside a UHV transmission electron microscope (TEM) chamber at a pressure of $< 1.5 \times 10^{-10}$ Torr. As far as the imaging resolution is concerned, the single-walled carbon nanotube (SWNT) should be the best for its unique sharpness [22, 23]. However, the surface morphology measurement always suffers from the quite flexible structure of a long SWNT. Fortunately, we can solve this problem by simultaneously using a more rigid MWNT as the tip base and *in situ* trimming the tip apex down to 5 nm, close to the dimension of a SWNT. The trimming is done by moving another STM sharp metal tip in the TEM to make contact with the tube end. When a voltage bias is applied to the STM tip, normally about 1 V, the contact area will be burned away due to the local heating. Moreover, as demonstrated in figure 1, we can first clean the AFM tip surface with the focused 200 keV e-beam. The heat generated will remove the amorphous layer coating the tip surface and thus minimize the contact resistance between the tip and the CNT inside the UHV chamber. This is to make sure that the applied voltage will reach the CNT in the EFM experiment. When a CNT-modified cantilever is used in the EFM, the convergence of the electrostatic field from the ultra-sharp CNT will help to enhance the resolution even though the tip is normally operated ~ 50 – 100 nm away from the sample. Besides, since the EFM is performed under the lift mode, it can avoid the strong contact occurring in the SSRM operation, and we do not need to worry about the inhomogeneous thickness of the coated insulator in SCM. All the *in situ* work was carried out in a JOEL JEM-2000V UHV TEM, using an acceleration voltage of 200 kV, with a three-dimensional (3D) ATTOCUBE stepper added to the chamber.

3. Sample description

The test sample used here is a chequerboard-like structure. After the shallow trench isolation (STI) etching and chemical mechanical polishing (CMP), SiO_2 gap fill was performed to give an array of $100 \times 100 \mu\text{m}^2$ silicon squares isolated by the STI of the same size. Photolithography and etching follow after another deposition of SiO_2 to result in gate-like structures on the silicon squares and STI areas, respectively. The SiO_2 gates serve as the implant hard mask for an implantation process of arsenic (As) at low energy (~ 2 keV), with a dose $\sim 10^{15} \text{ cm}^{-2}$. Typical thermal processes are applied after the implantation to activate the dopants. In figure 2(a), the black/white patterns in the SEM image correspond to the Si/ SiO_2 patterns. Figure 2(b) displays the multiple gate structure of our sample, which is composed of many sets of 3 or 5 narrow gates, namely the nanogates. Notice that there also exist wide microgates around $4 \mu\text{m}$ separating the nanogate sets. The cross-sectional SEM (XSEM) image in figure 2(c) demonstrates that the nanogate is about 40 nm wide and 100 nm high. The depth dopant profile (figure 2(d)) taken with a secondary ion mass spectrometer (SIMS) indicates that the buried dopant concentrations are much more than deep dopant concentrations, which confirms again that probing the plane view dopant profile is essential.

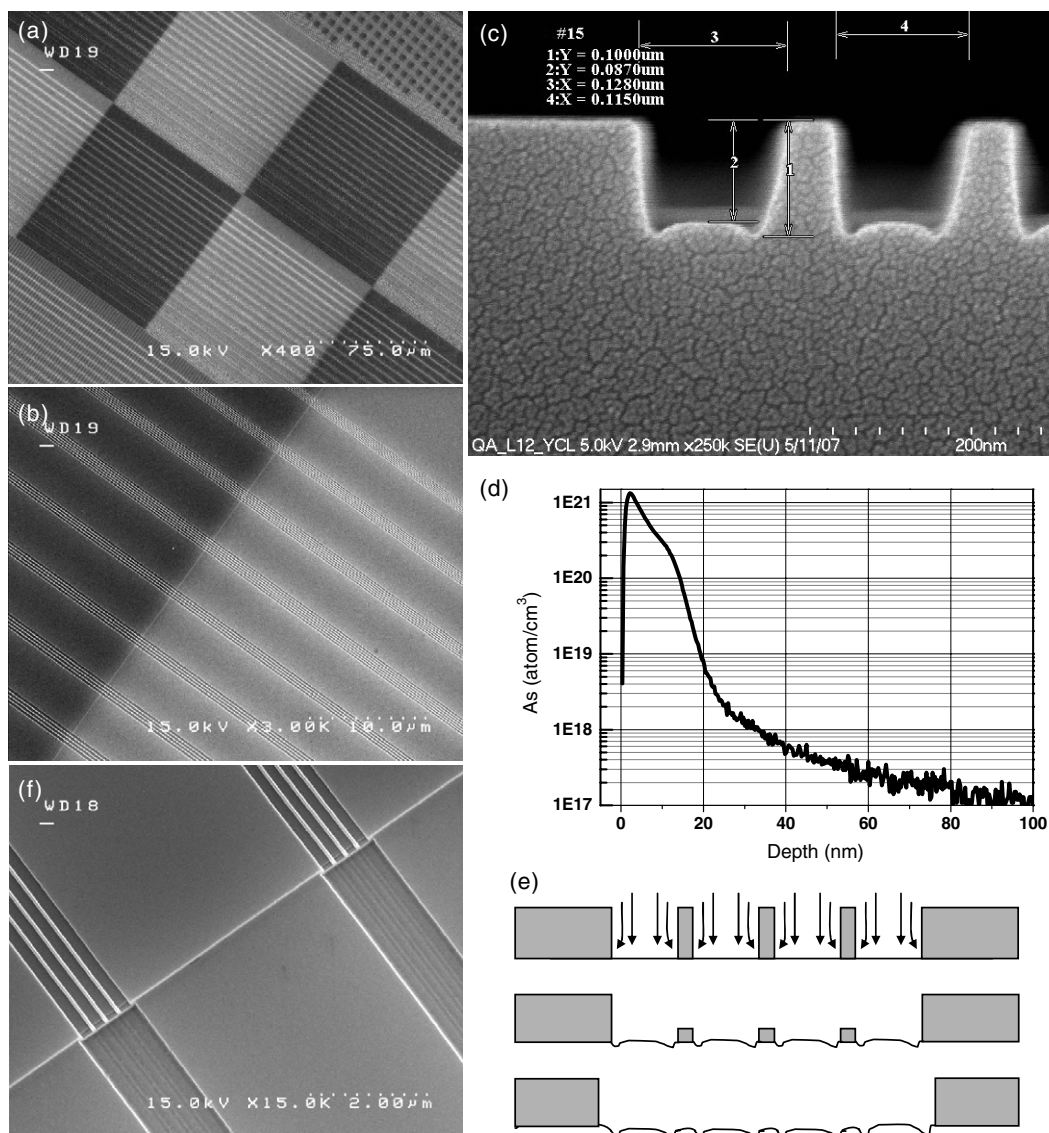


Figure 2. (a) A SEM image showing the black/white patterns corresponding to Si/SiO₂ patterns. (b) There are many sets of three or five roughly 50 nm wide nanogates within the patterns. The gate distances of the sets are different. Note that there are also 4 μm wide microgates between every nanogate set. (c) The cross-sectional SEM image shows that the gate width is less than 45 nm and the heights of all the gates are 100 nm. (d) The arsenic dopant depth profile taken with SIMS. (e) A scheme showing the isotropic etching of HF treatment. After being etched, the trenches will become broader and only doped Si remains under the gate regions. (f) The SEM image demonstrates the HF treated result, in which the SiO₂ gates are etched while the Si gates still exist. We are able to easily identify the areas of interest.

To obtain the plane view dopant profile, we etch the nanogates with an HF buffered solution of HF:water = 1:200 for 40–60 min. Generally, the nanogates are etched away at a faster rate than the microgates due to the sidewall HF etching. The scheme of such an isotropic etching is illustrated in figure 2(e). After being etched, the trenches will be slightly broadened, with the leftover microgates serving as the landmarks for areas of interest. A well HF treated result is demonstrated in figure 2(f) with very thin oxide layers left on the tops of nanogates. For the arsenic, implant energy is rather low, so we expect a lot of the doped Si areas exposed to HF to be etched away, and only the areas under the nanogates to remain doped. The detailed dopant profiles under the gate areas are investigated.

4. Electrostatic force microscopy results

All the EFM work operates with a secondary scan (or lift mode) associated with the primary tapping mode scan of AFM by a commercially available EFM/AFM system, Asylum Research MFP-3D, with maximum scan area size of 90 × 90 μm² and maximum piezotube resolved depth of 10 μm. During every line scan, the AFM and EFM operate successively, switching to the EFM just after every scan of AFM. In detail, the morphological information obtained by the AFM is stored in the primary scan, namely the topography. The secondary scan is performed following the topography exactly, only with the conductive tip lifted to a selected height with respect to the grounded sample. Since the lift mode scan is normally

operated with a voltage biased to the tip with the feedback loop open, the information acquired by the EFM maps out the surface potential of the sample. Our aim in this study is to use CNT-probed EFM to resolve the source/drain extension (SDE) under the gate areas. In a lift mode operation, the choice of height could bring some undesirable results to the secondary scan. In order to minimize the van der Waals interaction, series of height differences are ramped without a bias. Figure 3(a) is the AFM image formed by the primary scan, revealing the surface morphology in figures 2(e) and (f). We ramp the height from 0 to 90 nm (as indicated) to take the EFM phase image without bias in figure 3(b). Apparently, it displays no signal after the CNT tip is lifted to 70 nm. This height is thus chosen for the following EFM experiment and the phase image is shown in figure 3(c). This image, without any bias, shows no clear signal from the doping information, as expected. The hardly noticeable slight signal coincident with the morphology is due to the inertial change of phase, which results from disabling the feedback response when the EFM follows the topography across an abrupt edge. Here, we only focus our measurement on the EFM phase signal because it is more sensitive than the amplitude change.

It has been proved that the phase of the tapping cantilever in AFM is related to the material properties [24, 25]. One of these properties is related to the local doping density [26, 27]. Hence, we map the dopant distribution under the gate area by EFM phase measurements with the CNT tip biased at 1, 2, 3, and 4 V, displayed in figures 4(a)–(d), respectively. We can see that the phase contrast becomes sharper and the dopant profile gradually broadened as the tip bias increases. Of all different biased EFM images, figure 4(c) seems to have the best contrast while figure 4(d) displays a broader dopant distribution, which may have resulted from the contribution of deeper dopants. When the bias is raised higher than 5 V (as displayed in figure 4(e) with the ramped bias from 5 to 10 V), the EFM image is apparently afflicted with abrupt broadening and flicks on the dopant distribution. Coexistence of these two phenomena strongly suggests that the nanotube tip become unstable under high electric field. The EFM phase images illustrate that slight SDE does not lead to the overlap of the source/drain (S/D) regions. The EFM phase image taken with a commercial conductive tip biased at 3 V also shows the distinguished dopant distribution at the nanogate region (figure 4(f)). However, in contrast to figure 4(c), the spatial resolution of the EFM image is so poor that not only is the gate's physical image blurred, the dopant distribution, i.e. the plane view SDE, is also broadened since the electrical field defined by a commercial tip is much more divergent. It is impossible to extract the exact effective channel length using this image, especially when the nanogate length is going down to less than 50 nm.

For convenience, we pick the EFM phase image taken with the 3 V biased CNT tip (figure 4(c)) to discuss SDE in detail for the ratio of line edge roughness and line width roughness (LER/LWR). Figure 5(a) converts the grey scale of figure 4(c) into colour. Figure 5(b) is a software-aided drawing about L_{eff} variations deduced from figure 5(a), which will be discussed in detail in the next paragraph. In figure 5(b)

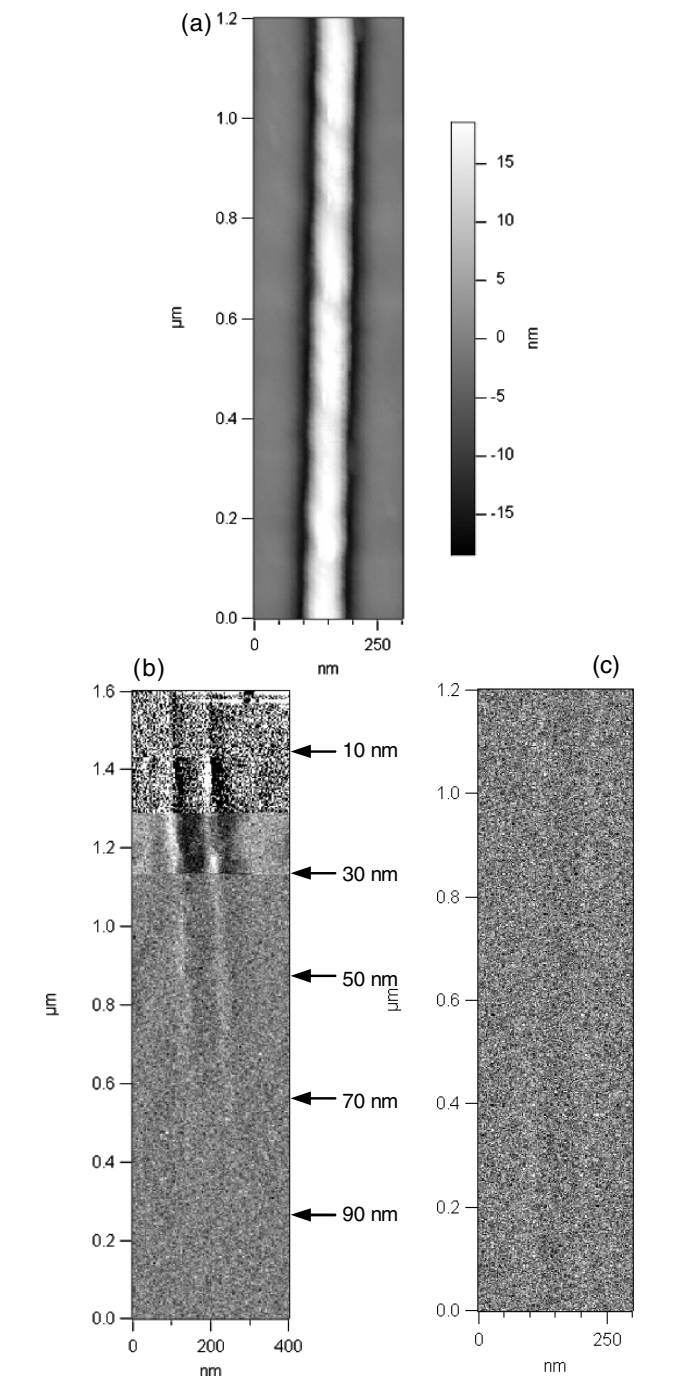


Figure 3. (a) The AFM image formed by the primary scan. It also shows the surface morphology after HF treatment. (b) The EFM phase image without bias by ramping the height difference. 70 nm seems to be the minimum height at which the Van der Waals interaction disappears. (c) The EFM phase image taken at 70 nm high without bias displays no clear contrast. The slight signal similar to (a) is due to the inertial effect.

the L_{eff} variations (red lines) show the channel roughness of 10 nm, which approaches the results obtained by the UHV STM presented before [10]. In figure 5(a), L_{eff} is uniform in most of the regions under the gate but it seems that the stronger SDEs marked by the white lines might induce critical overlaps in this device. To make sure that this did not happen, we took

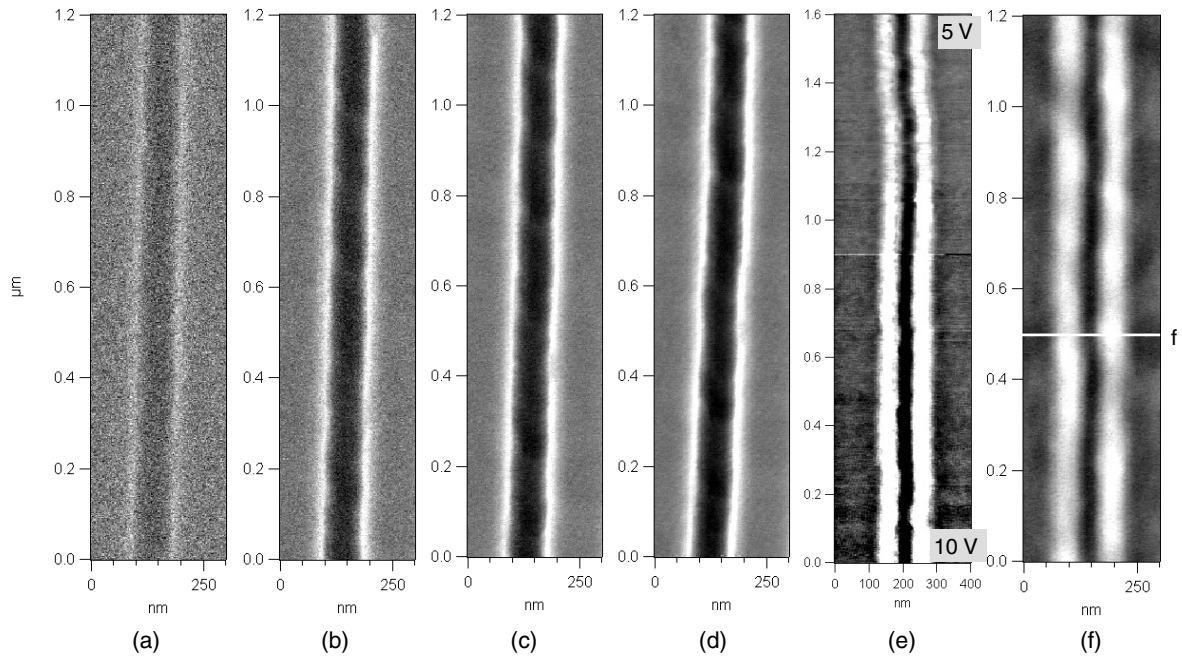


Figure 4. (a)–(d) correspond to the EFM phase image taken with the CNT tip bias at 1–4 V. The phase contrast becomes sharper as the tip bias increases. (e) The EFM phase image with ramped bias 5–10 V appears more noisy. Of all biases, 3 V seems to be the choice offering the best image quality. The SDE is slight and no overlap between the S/D happens. (f) EFM phase image taken with a commercial conductive tip at a bias of 3 V, showing poor resolution in comparison with (c).

three line scans at some critical local regions in figure 5(a), marked as c, d, and e, and the data are depicted in figures 5(c)–(e), respectively. Apparently, no dopant information appears in the central part of the gate area for all three line scans. In comparison, the line scan marked as f in figure 4(f), taken with a commercial conductive tip, shows a broader dopant profile, which could give rise to an incorrect interpretation of the S/D overlap.

After the examination of the S/D overlap, another critical question is whether the lateral roughness of L_{eff} defined by the SDE profile follows the line edge roughness (LER). Previous studies have paid much attention to analysing the device performance under the assumption of L_{eff} being defined by the LER. However, more recent SCM [15–17], SSRM [7, 9], and STM [11, 12] results all show asymmetric cross-sectional dopant profiles, which indicates that the previous assumption is not correct. In 2004, Xiong and Bokor disclosed their simulation results which showed that the dopant diffusion's root-mean-square (RMS) value was quite different from the LER/LWR ratio, and it was predominantly the dopant profile that contributed to the device performance [28]. This was experimentally proved by Fukutome *et al* in 2006 with the 2D plane view dopant profile obtained by UHV STM [10]. In figure 5(b), we trace the nanogate boundaries with the raw data of figure 3(a) by mapping the line shape of the two shallow trenches (as the black lines indicated). In fact, figure 3(a) is the primary AFM image of figure 5(a). However, these traced boundaries are somehow incorrect because the isotropic HF etching has destroyed the original ones. Technically speaking, we can only approximately regard the shallow trenches as the nanogate boundaries revealing the LER, although the line

width is broader than the XSEM image shown in figure 2(c). In section 3, we claim that our sample is fabricated in a sub-45 nm CMOS process. If we look at figure 2(c), we can find the bottom parts of the nanogates close to 50 nm wide. The red lines, representing the L_{eff} boundaries, were deduced from the raw data of the EFM phase image in figure 5(a). We drew the boundaries of the phase value $<95.3^\circ$, which corresponds to the deep blue regions in figure 5(a). The L_{eff} in figure 5(b) varies from 25–45 nm unlike the traced nanogate boundaries (black lines). Obviously, the SDE profile demonstrates that no S/D overlap occurs in this device but there is a fluctuating L_{eff} . We again successfully resolve the LER and SDE profiles to 10 nm and prove that the lateral line shape of L_{eff} is different from the LER.

5. Conclusion

In conclusion, the EFM plane view dopant profiling methodology is greatly enhanced by our *in situ* modified CNT tip, especially resolving the dopant features to within 10 nm in air. From all the EFM images in figures 4 and 5, dopant diffusions around the source and drain (S/D) regions for our samples are found not to be serious. The line scans taken at some critical regions in figure 5(a) unambiguously eliminate concern about the possible electrical connections between the S/D regions of the device. In addition, we demonstrate that the SDE and LER profiles are not coincident. The EFM measurements with the simple HF treatment are easy to operate in air without complicated sample preparations. We demonstrate in this work that the EFM employing the CNT-

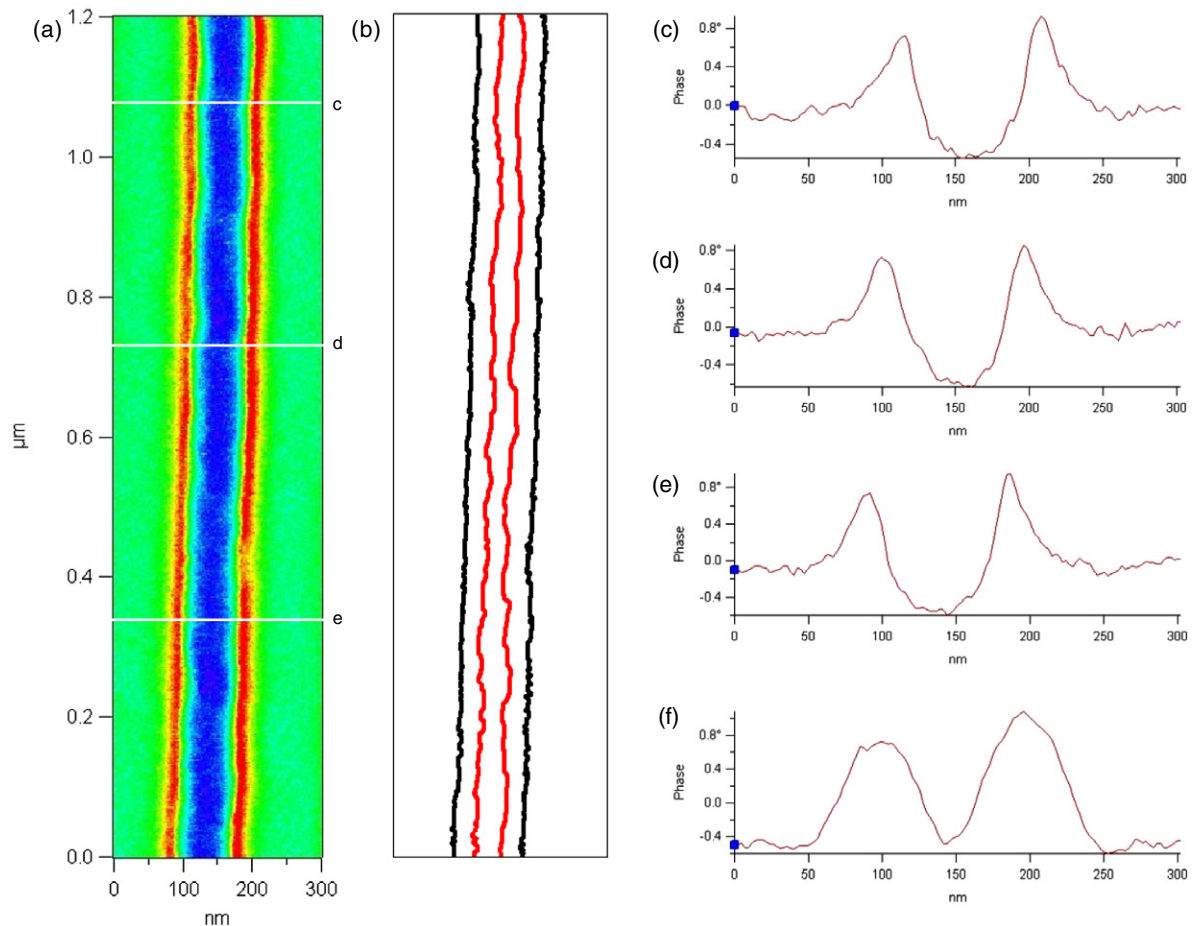


Figure 5. (a) The colour display transformed from figure 4(c), resolving dopant features to 10 nm. (b) The SDE profile (red lines) shows that the L_{eff} variations, of around 25–45 nm, are not the same as the LER (black lines). The resolution of 10 nm can be proved by the L_{eff} roughness appearing within the red lines. (c)–(e) The line scans taken at three critical regions across the nanogate in (a) again show no apparent S/D overlap. (f) The line scan taken from figure 4(f) for comparison.

modified cantilever can serve as a good characterization tool for sub-45 nm device fabrication.

Acknowledgments

The authors would like to thank Wei-Bin Su, Ing-Shouh Hwang, Hsien-Shun Liao, Po-Yen Lin, Wei-Chao Lai, Yu-Sheng Ou, and Yi-Ru Chang in IPAS and An-Chun Chien in WUSTL for their helpful discussions and suggestions. This work is supported by the 2007 AS-TSMC joint project.

References

- [1] Mukhopadhyay S, Kim K and Chuang C T 2008 *IEEE Trans. Electron Devices* **55** 152
- [2] Frank D J, Taur Y, Ieong M and Wong H S P 1999 *Symp. VLSI Tech. Dig.* p 171
- [3] Asenov A 1998 *IEEE Trans. Electron Devices* **45** 2505
- [4] Bhavnagarwala A, Tang X and Meindl J D 2001 *IEEE J. Solid-State Circuits* **36** 658
- [5] ITRS Website: <http://public.itrs.net>
- [6] De Wolf P, Snauwaert J, Hellemans L, Clarysse T, Vandervorst W, D'Olieslaeger M and Quaeysaegens D 1995 *J. Vac. Sci. Technol. A* **13** 1699
- [7] Eyben P, Alvarez D, Jurczak M, Rooyackers R, De Keersgieter A, Augendre E and Vandervorst W 2004 *J. Vac. Sci. Technol. B* **22** 364
- [8] Álvarez D, Fouchier M, Kretz J, Hartwich J, Schoemann S and Vandervorst W 2007 *Microelectron. Eng.* **73/74** 910
- [9] Álvarez D, Hartwich J, Fouchier M, Eyben P and Vandervorst W 2003 *Appl. Phys. Lett.* **82** 1724
- [10] Fukutome H, Momiyama Y, Kubo T, Tagawa Y, Aoyama T and Arimoto H 2006 *IEEE Trans. Electron Devices* **53** 2755
- [11] Fukutome H, Momiyama Y, Tagawa Y, Kubo T, Aoyama T, Arimoto H and Nara Y 2005 *Symp. VLSI Tech. Dig.* p 140
- [12] Fukutome H, Aoyama T and Arimoto H 2005 *Japan. J. Appl. Phys.* **44** 2395
- [13] Gupta S, Williams O A and Bohannon E 2007 *J. Mater. Res.* **22** 3014
- [14] Girard P 2001 *Nanotechnology* **12** 485
- [15] Kimura K, Kobayashi K, Matsushige K, Usuda K and Yamada H 2007 *Appl. Phys. Lett.* **90** 083101
- [16] Chao K J 2006 *J. Vac. Sci. Technol. B* **24** 390
- [17] Williams C C, Slinkman J, Hough W P and Wickramasinghe H K 1989 *Appl. Phys. Lett.* **55** 1662
- [18] Dai H, Hafner J H, Rinzler A G, Colbert D T and Smalley R E 1996 *Nature* **384** 147

- [19] Chang Y C, Wang D C, Chang C S and Tsong T T 2003 *Appl. Phys. Lett.* **82** 3541
- [20] Tzeng S D, Wu C L, You Y C, Chen T T, Gwo S and Tokumoto H 2002 *Appl. Phys. Lett.* **81** 5042
- [21] Arnason S B, Rinzler A G, Hudspeth Q and Hebard A F 1999 *Appl. Phys. Lett.* **75** 2842
- [22] Wilson N R and Macpherson J V 2004 *J. Appl. Phys.* **96** 3565
- [23] Cheung C L, Hafner J H and Lieber C M 2000 *Proc. Natl Acad. Sci. USA* **97** 3809
- [24] Cleveland J P, Anczykowski B, Schmid A E and Elings V B 1998 *Appl. Phys. Lett.* **72** 2613
- [25] Zhong Q, Inniss D, Kjoller K and Elings V B 1993 *Surf. Sci.* **290** L688
- [26] Nelson M W, Schroeder P G, Schlaf R and Parkinson B A 1999 *J. Vac. Sci. Technol. B* **17** 1354
- [27] Lei C H, Elliott M and Macdonald J E 2004 *Nanotechnology* **15** 627
- [28] Xiong S and Bokor J 2004 *IEEE Trans. Electron Devices* **51** 228